Rapid, non-invasive fluorescence margin assessment: Optical specimen mapping in oral squamous cell carcinoma

Stan van Keulen[a,c], Nynke S. van den Berg[a], Naoki Nishio[a], Andrew Birkeland[a], Quan Zhou[a], Guolan Lu[a], Han-Wei Wang[b], Lyle Middendorf[b], Tymour Forouzanfar[c], Brock A. Martin[d], A. Dimitrios Colevas[e], Eben L. Rosenthal[a,*]

[a] *Department of Otolaryngology, Stanford University School of Medicine, 900 Blake Wilbur Drive, Stanford, CA 94305, United States*
[b] *LI-COR Biosciences, 4647 Superior St, Lincoln, NE 68504, United States*
[c] *Department of Oral and Maxillofacial Surgery/Oral Pathology, VU University Medical Center/Academic Centre for Dentistry Amsterdam (ACTA), Amsterdam, the Netherlands*
[d] *Department of Clinical Pathology, Stanford University School of Medicine, 300 Pasteur Dr, Palo Alto, CA 94304, United States*
[e] *Department of Medicine, Division of Medical Oncology, University School of Medicine, 269 Campus Drive, Stanford, CA 94305, United States*

ARTICLE INFO

ABSTRACT

Objective: Surgical resection remains the primary treatment for the majority of solid tumors. Despite efforts to obtain wide margins, close or positive surgical margins (< 5 mm) are found in 15–30% of head and neck cancer patients. Obtaining negative margins requires immediate, intraoperative feedback of margin status. To this end, we propose optical specimen mapping of resected tumor specimens immediately after removal.
Materials and methods: A first-in-human pilot study was performed in patients (n = 8) after infusion of fluorescently labeled antibody, panitumumab-IRDye800 to allow surgical mapping of the tumor specimen. Patients underwent standard of care surgical resection for head and neck squamous cell carcinoma (HNSCC). Optical specimen mapping was performed on the primary tumor specimen and correlated with pathological findings after tissue processing.
Results: Optical mapping of the specimen had a 95% sensitivity and 89% specificity to detect cancer within 5 mm (n = 160) of the cut surface. To detect tumor within 2 mm of the specimen surface, the sensitivity of optical specimen mapping was 100%. The maximal observed penetration depth of panitumumab-IRDye800 through human tissue in our study was 6.3 mm.
Conclusion: Optical specimen mapping is a highly sensitive and specific method for evaluation of margins within < 5 mm of the tumor mass in HNSCC specimens. This technology has potentially broad applications for ensuring adequate tumor resection and negative margins in head and neck cancers.

Introduction

Surgical resection remains the gold standard for the majority of solid tumors [1]. Despite improved medical technologies for preoperative surgical planning [2,3] and intraoperative guidance, including radio-guided and fluorescence imaging-based approaches [4,5], head and neck surgeons still primarily rely on their vision and palpation to determine surgical margins. Not surprisingly, tumor-positive margins are still found in 15–30% of all head and neck cancer resections [6–8]. In head and neck cancer, a positive margin is defined as tumor within 2 mm of the cut edge, and a close margin is defined as tumor tissue 2–5 mm from the cut edge. Importantly, positive margin status is directly correlated with locoregional residual cancer and overall survival [9–11]. Although controversial and situation dependent, both close and positive margins are often clinically treated similarly, with recommendations for further resection to achieve negative margins. However, as margins are not definitively established until final pathology reports are issued many days after surgery, re-resection can be challenging clinically and can add morbidity to the patient's care. Immediate assessment of the specimen's margins in the operating room would provide immediately actionable information to the surgeon.

The current standard for detecting residual disease is gross

* Corresponding author at: Department of Otolaryngology, 900 Blake Wilbur Drive, Stanford, CA 94305, United States.
E-mail addresses: stanvk@stanford.edu (S. van Keulen), nsvdb@stanford.edu (N.S. van den Berg), nn240@stanford.edu (N. Nishio), abirkela@stanford.edu (A. Birkeland), qzh@stanford.edu (Q. Zhou), guolanlu@stanford.edu (G. Lu), brockm@stanford.edu (B.A. Martin), elr@stanford.edu (E.L. Rosenthal).

inspection of the surgical specimen and/or wound bed, followed by frozen sectioning of suspicious areas for further histopathological assessment [12]. Besides the time-consuming nature of the procedure (15–20 min per frozen section), frozen section analysis can only examine a small fraction of the specimen [12]. Another limitation of frozen section analysis is the risk of sampling error, which may be further impaired by the limited ability of the surgeon to predict and thus select areas with tumor involved margins [15,16]. In order to overcome these limitations, we propose a technique that allows real-time intraoperative evaluation of the entire surface of the resected specimen to preselect "at risk" margins using an optical scanning technique.

Using systemically administered near-infrared (NIR) dye labeled tumor targeting antibodies, we and others demonstrated that the fluorescent signal detected in tumor tissue is much higher than surrounding normal tissue [16–19]. The NIR fluorescence can penetrate through approximately 5–6 mm of tissue, allowing for precise identification of tumor and normal tissue. The goal of the current study was to understand if the properties of NIR light can be used clinically to identify close margins and quantify the distance between the specimen's surface and the depth of the tumor mass. We hypothesize that with macroscopic optical specimen mapping (OSM) of the whole surgical specimen, we can accurately predict close and/or positive tumor margins. This OSM technique will allow the surgeon to evaluate the entire surface of the specimen for suspicious areas that need further assessment using frozen sectioning in order to achieve a complete oncological resection.

Materials and methods

Optical specimen mapping device

The OSM device (IGP-ELVIS, LI-COR, Lincoln, NE, USA) provides an enclosed ambient light-free space for consistent and reliable closed-field fluorescence imaging. Inside the closed-field space, a motion and rotational stage offers a variety of view angles of the specimen within an imaging sequence along two rotational axes. To achieve OSM, motion stages in the chamber were synchronized with the excitation and detection components in the optical module. Fig. 1 provides an overview of the device used for OSM of the deep surface of the tumor. The imaging volume is formed by the illumination light field together with the depth-of-focus and the field of view of the imaging lens (Fig. 1b). The controlled light sources comprise laser diodes at 785 nm and visible white light LEDs. Illumination is below the maximum permissible exposure (ANSI Z136.1-2007) so the specimen is not damaged by the light. The imaging resolution of the device was about 100 LP/in. (125 µm) within the imaging volume of 500 mL. Imaging at a higher resolution of 150LP/in. (85 µm) is available for small samples under 50 mL. The fluorescence images were collected through an 800 nm channel with center wavelength at 820 nm. A control program (based on LabVIEW, National Instrument, TX, USA) ran the imaging process connected to a customized Image Studio software (LI-COR Biosciences) for imaging collection, storage, and analysis.

Establishing imaging parameters

To determine the maximal fluorescence penetration depth of IRdye800CW-carboxylate and to test the three-dimensional surface mapping functionality, a tissue-mimicking phantom with homogenous IRdye800CW-carboxylate distribution was created in 1% agarose (Life Technologies, Carlsbad, CA, USA), 1% whole bovine blood (Sigma-Aldrich, Saint Louis, MO, USA) and 1% intralipid emulsion (Sigma-Aldrich) [17]. First, the agarose in water solution was heated to 80 °C and allowed to cool down to 45 °C before adding bovine blood, intralipid and IRDye800CW-carboxylate (916 nM) under continuous stirring to ensure homogeneous distribution. The concentration of

IRDye800CW used in the phantom was selected to be clinically-relevant by matching the fluorescence with tumor samples from patients. Hereafter, the mixture was poured into cube shaped molds (12.7 × 12.7 × 12.7 mm; volume: 2.0 mL) and cooled down to solidify. The phantom was then imaged with the OSM device, after which increasing stacks of bovine muscle (thin sliced ribeye) were placed over the phantom (Fig. 3). Upon increasing stacks, the phantom was re-imaged on the device whereby the thickness of stacks was measured by taking the average of three measurements of all stacked layers. Quantitative analysis of the images was performed using Image Studio (LI-COR Biosciences) by drawing regions of interest (ROIs) in the middle of the phantom and extracting the mean fluorescence intensity (MFI). The MFI was then plotted against the depth (i.e. thickness) of all overlaying non-fluorescent muscle stacks. Signal-to-noise ratios were calculated by dividing the $MFI_{phantom}$ and $MFI_{background}$ (region next to phantom).

Clinical study

Study design

Prior to enrollment, written informed consent was obtained from all patients. The Phase I study evaluating panitumumab-IRDye800CW was approved by the Stanford Institutional Review Board (IRB-35064) (NCT02415881). More details on the phase I study can be found in Gao et al. [19]. Briefly, patients (n = 8) were infused 1–4 days prior to surgery with a flat dose of 25 mg (n = 4) or 50 mg (n = 4) panitumumab-IRDye800CW (excitation/emission max: 774/789 nm; half-life: 24 h [19]). After resection, the tumor specimens were imaged with the OSM device before being sent to pathology for standard of care histological assessment. There, the specimen was formalin-fixed and cut in 5 mm tissue sections. The specimen was then reconstructed from the 5 mm sections and re-imaged. Thereafter, the 5 mm tissue sections were processed and paraffin-embedded. From each 5 mm section, a representative 5 µm section was cut for routine hematoxylin and eosin (H &E) staining for diagnosis. On the acquired H&E slides, areas with invasive or *in situ* SCC were outlined by a board-certified pathologist. The slides were then digitized and analyzed for our study.

Correlation of fluorescence signal with margin distance

To assess the fluorescent signal, a binary yes/no approach was used by placing a raster (5 × 1 mm) over the lateral side of the imaged specimen. Similar to the approach previously described [16,19–22], the threshold was adjusted for each specimen to reveal heterogeneity in fluorescence intensity within the gross tumor and no signal in normal tissue (i.e. muscle, fat). Areas on the surface exceeding the threshold within the raster were considered positive for fluorescence, and areas below the threshold were considered negative for fluorescence. On the digitized outlined H&E slides, we used ImageJ (version 1.50i, National Institute of Health, Washington D.C., Maryland, USA) to measure the distance from the tumor border to the specimen's edge, further defined as *margin distance* (Fig. 2). This *margin distance* for fluorescence positive areas was then compared to the *margin distance* for fluorescence negative areas using an unpaired, two-tailed *t*-test. To determine the sensitivity and specificity of OSM for tumor detection on the deep surface, a receiver operation characteristic (ROC) curve was generated. Values were reported as means with standard deviation and 95% confidence intervals (95%CI) where applicable. False-positive results were specified as an area positive for fluorescence but negative for tumor within 5 mm from the specimen's edge; false-negative results were defined as an area negative for fluorescence but positive for tumor within 5 mm of the specimen's edge.

Results

Optical specimen mapping validation

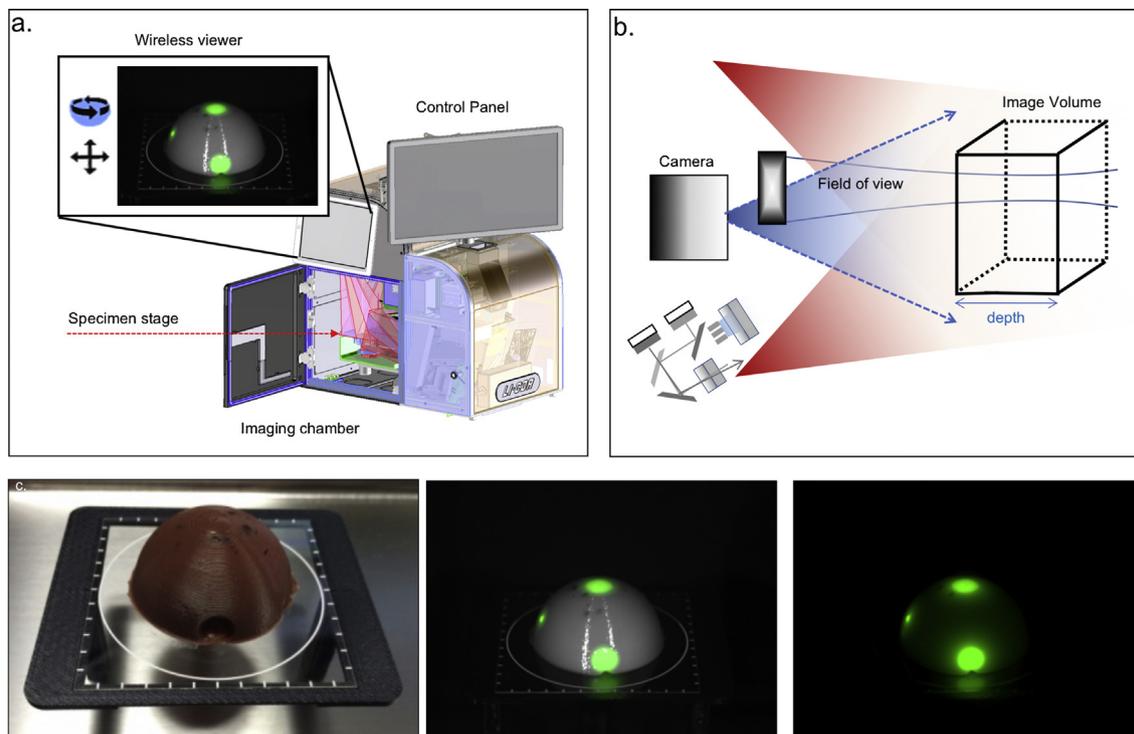In order to validate optical scanning as a means to predict the

Fig. 1. Fluorescence Optical Specimen Mapping Device. The device is an instrument for sensitive and consistent specimen mapping (specimen sizes up to 10 cm × 10 cm). The fluorescence images can be assessed through two wireless viewers. One of the viewers is mounted on the device, the other can be detached from the device and allows the user to view the images in another room or building. (a). Schematic drawing of the illumination light (red beams) and the imaging volume, which is formed by the illumination light fields, imaging depth-of-focus and field of view of the imaging lens (b). Optical phantom with dye plugs (c). First, a bright field image, second an overlay of fluorescence and white light image and third a fully fluorescence image. (For interpretation of the references to colour in this figure legend, the reader is referred to the web version of this article.)

distance between the tumor border and cut specimen edge (the *margin distance*), we conducted a phantom study using physiologically relevant concentrations of the dye in the phantom and fresh bovine tissues. An IRDye800CW loaded tumor phantom (tissue-mimicking lipid and blood mixture) was imaged in the optical scanner using a concentration of dye consistent with what we found in the tumor specimens obtained during the clinical trial. OSM was performed using incremental thickness of normal tissue to determine the maximal distance at which the fluorescent signal was still detectable. Fig. 3 shows the visual appearance of the phantom experiment. The signal-to-noise ratio ($MFI_{phantom}$ divided by $MFI_{background}$) of the non-stacked phantom was found to be 253 (Fig. 3). The penetration depth of IRDye800CW signal though unloaded muscle layers was 11 mm (lowest signal-to-noise ratio 1.2 ± 0.1).

Clinical study

Optical surface mapping of the specimen

OSM was performed on the back table in the operating room in parallel with the surgery. After the surgeon had removed the primary tumor specimen from the patient, it was imaged directly in the OSM device whereby the deep margin side was positioned upwards (i.e. facing the camera). There were no issues with specimen positioning. The acquisition time for a two-dimensional top view image was around 25 s (1 image) and 7 min (17 images) for a full three-dimensional optical specimen map. By scaling the fluorescence threshold, suspicious regions could easily be recognized on the specimen to be further interrogated by the surgeon based on clinical judgement. As the device captured both white-light images and fluorescent images simultaneously, we were able to project the white-light channel over the fluorescence
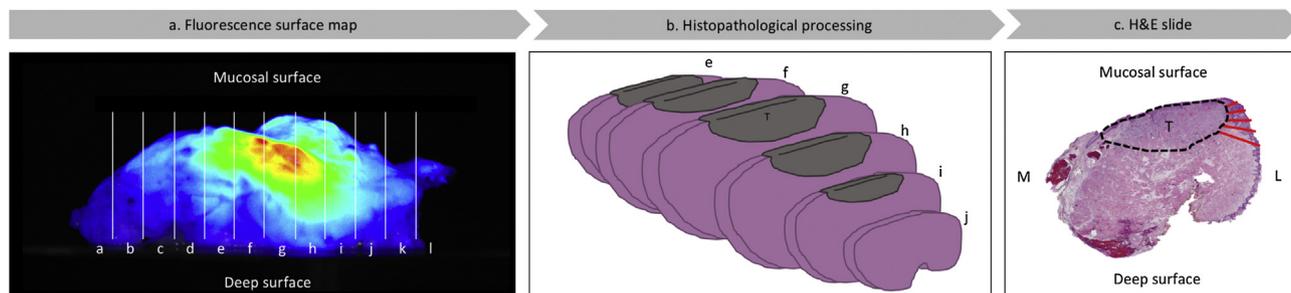

Fig. 2. Flow diagram of optical surface mapping analysis. Lateral side view of representable specimen (buccal) (a) which was formalin fixed, sectioned in 5 mm serial sections (white lines) (b). Tumor areas were outlined (black dashed line) on the H&E slides and *margin distances* (red lines) were measured at 1 mm intervals (c). Consequently, the number of measurements was defined by the maximal tumor depth as measured from the mucosal surface to the deep surface on the H&E slide. *Margin distances* in fluorescence areas were compared to *margin distances* in areas without fluorescence. T = tumor tissue; M = medial; L = lateral; H&E slide = Hematoxylin and eosin slide. (For interpretation of the references to colour in this figure legend, the reader is referred to the web version of this article.)
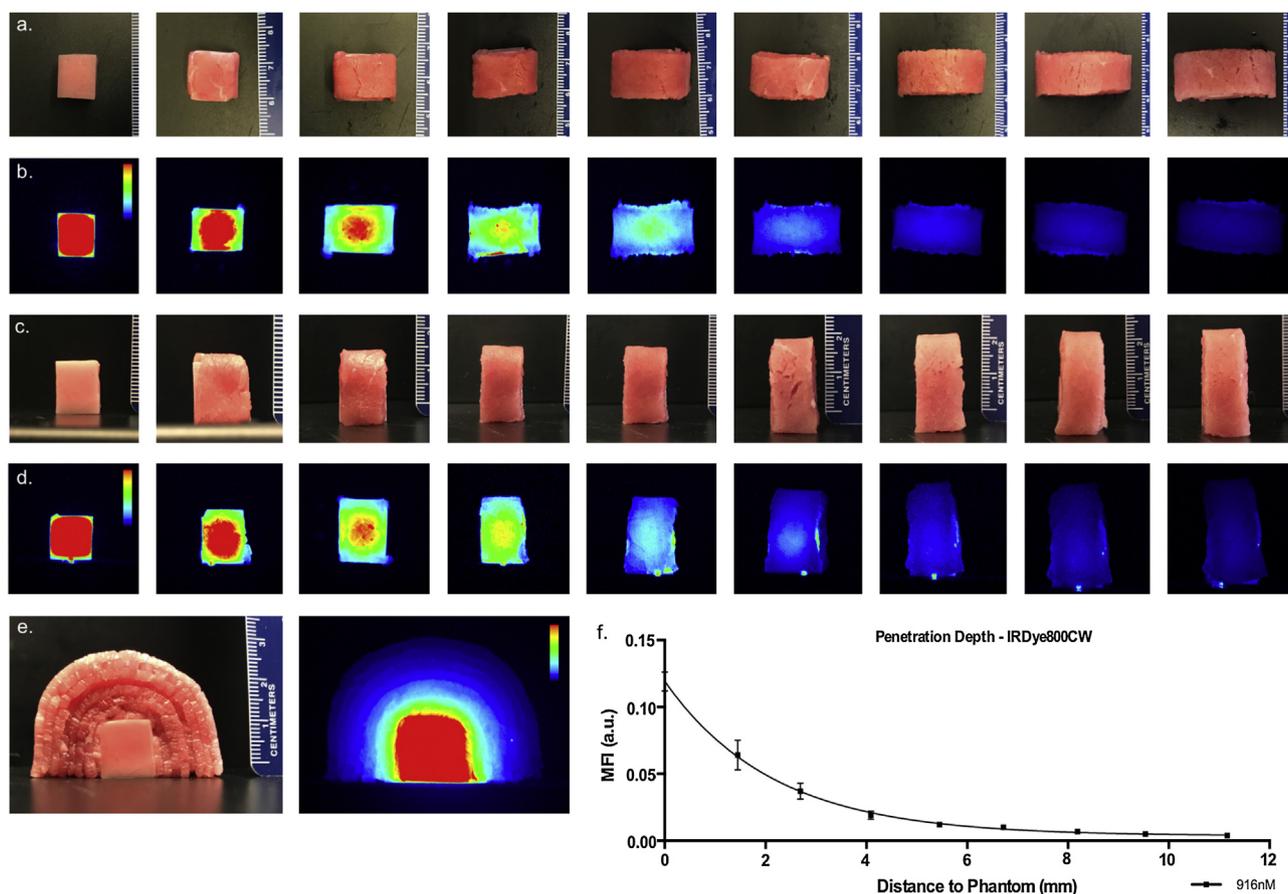
Fig. 3. Penetration depth of fluorescence for IRDye-800CW loaded phantom. Visual presentation, of two series of representative bright field and corresponding fluorescence images (first image without stacking, second image is one layer, third image two layers, etc.) that show the decrease in fluorescence signal as the distance to the phantom increases. Row (a) and (b) were imaged by the top view camera, row (c) and (d) were imaged with the side view camera. Informative bright field and corresponding fluorescence image of side view on phantom (e). Quantitative analysis of the fluorescence signal with increasing distance to the phantom (f). Color bars are given were applicable.

channel to further "isolate" suspicious areas. Consequently, data interpretation was intuitive for the surgeon since specific landmarks could be identified on the specimen and suspicious areas rapidly located on the specimen. Location within the operating room was considered by the surgeon to be optimal for immediate assessment and specimen orientation.

Fluorescence signal vs. margin distance

To determine if OSM could predict close (< 5 mm) or positive (< 2 mm) margins, we performed optical scanning of the primary tumor specimens of eight consecutive patients with HNSCC (Table 1). Of these eight patients, six were eligible for analysis using our methodology (see Table 1 for details). Fig. 4 shows a representative example of an optical surface map that was generated from a patient with lateral tongue cancer.

Following serial sectioning of the surgical specimens, a total of 39 sections contained tumor tissue, and a total of 160 data points were extracted. As shown in Fig. 5a–e, the presence or absence of fluorescence on the specimens' surface correlated with the presence or absence of tumor close to the specimen's margin. Specifically, when a fluorescence signal was present on the deep surface of the specimen, tumor was significantly closer to the edge than when no fluorescence signal was detected (2.6 ± 0.1 mm versus 6.9 ± 0.2 mm, respectively; $p < 0.0001$; n = 160).

Sensitivity and specificity of optical surface mapping

Sensitivity and specificity of OSM for tumor detection were

Table 1
Patient and tumor characteristics.

Age	Gender	Tumor location	pTNM
54	M	Buccal mucosa[*]	T2N0M0
48	M	Lateral tongue	T3N2cM0
71	M	Lateral tongue	T2N0M0
58	F	Retromolar trigone[**]	T3N0M0
65	F	Buccal mucosa	T2N2bM0
71	F	Buccal mucosa	T3N0M0
63	F	Palate	T2N0M0
71	F	Lateral tongue	T2N2bM0

[*] The first patient (SCC of the buccal mucosal tissue) was excluded as the fluorescence signal was a factor 10 lower (MFI = 0.025) than the other patients (MFI = 0.25). It is likely that the reduced signal is caused by the prolonged time of infusion to surgery of the panitumumab-IRDye800CW compared to the other patients (92 h versus 21 h average).

[**] Another patient with SCC of the retromolar trigone was excluded. Although the tumor could be imaged successfully in the OSM device, the exophytic nature of the tumor prevented three-dimensional pathological reconstruction of the specimen. This reconstruction is needed for accurate analysis of the margin distances and therefore the patient was excluded.

determined using a ROC curve (Fig. 5g). Optical specimen mapping achieved high sensitivity regardless of cut-off *margin distances*. In particular, at the < 5 mm cut-off distance (clinically defined as close or positive margin), positive fluorescence status was highly sensitive and specific (95% and 89%, respectively). In addition, fluorescence was able to detect 100% of cancer tissue within < 2 mm of the surgical
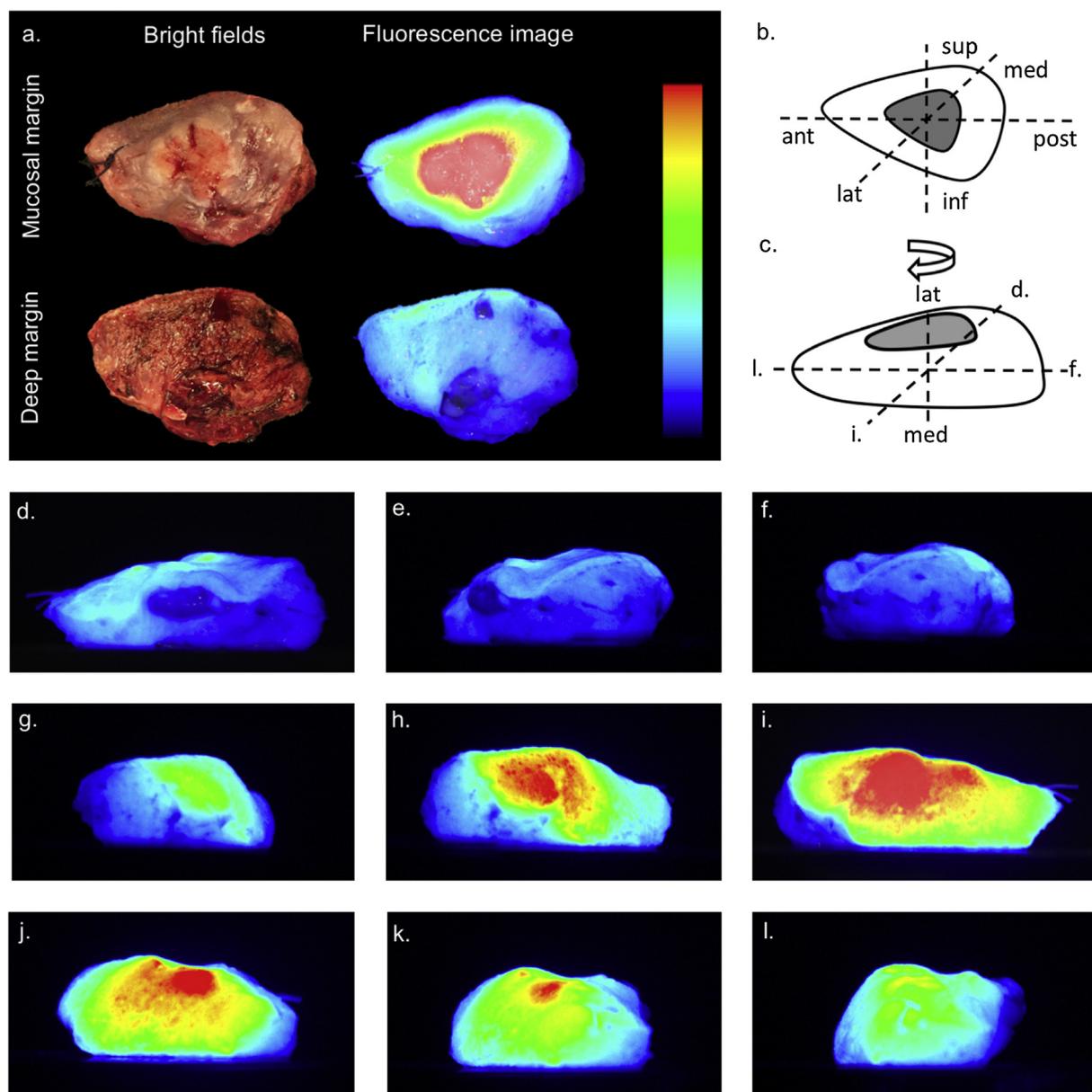
Fig. 4. Optical specimen map of representable patient. Optical specimen mapping of a surgical specimen from a patient who underwent a hemiglossectomy. Bright field and fluorescence images of mucosal margin and deep margin (a) with anatomical orientation of resected surgical specimen in the oral cavity (b). Color bar indicates the threshold settings. Furthermore, the rotational views of the specimen (d–l) with illustration (c) indicating the rotational direction and corresponding views (d, i, f and l). Interactive animation allows the user to scroll through the tumor-surface map (along multi-axis) and pause at a specific view for detailed inspection. Note that this figure contains merely a representative selection of 11 from the 22 images that make up the three-dimensional rendering. sup = superior; inf = inferior; ant = anterior; post = posterior; med = medial; lat = lateral.

resection margin (i.e. true positive margins). At the 2–5 mm range (close margin range) the sensitivity was 95–100%. Notably, specificity was lower at the < 2 mm range and the 2–5 mm range (1–41% and 41–89%, respectively). The area under the curve (AUC) was 0.97 using the 5 mm cut-off (p < 0.0001, n = 160). From all 160 data points, false-positive results (i.e. fluorescence positive edge, but tumor distance > 5 mm) were found in 7% of all fluorescence positive margins, whereas 2% of all fluorescence negative margins resulted in false-negative findings (i.e. fluorescence negative edge, but tumor distance < 5 mm).

Penetration depth of panitumumab-IRDye800

While the penetration depth of fluorescent signal in an ideal phantom set-up reached a maximum of 11.0 mm (Fig. 2), in human tissue the maximal observed penetration depth of panitumumab-

IRDye800 was 6.3 mm; at higher *margin distances*, 100% of the overlying surface remained negative for fluorescence signal, whereas at distances < 6.3 mm fluorescence signals could be detected.

Discussion

Although frozen section examination has shown to be highly accurate (90%) if performed by an experienced pathologist [15], only a small fraction of the specimen can be sampled with identification of suspicious areas based on visual inspection and palpation. This may, amongst other factors, contribute to the large portion of positive margins (15–30%) still found in all HNSCC resections at permanent pathological analysis [6–8,13]. Here we demonstrate that the use of optical mapping may allow identification of high-risk areas on the surgical specimen that need further evaluation using clinical judgment or frozen
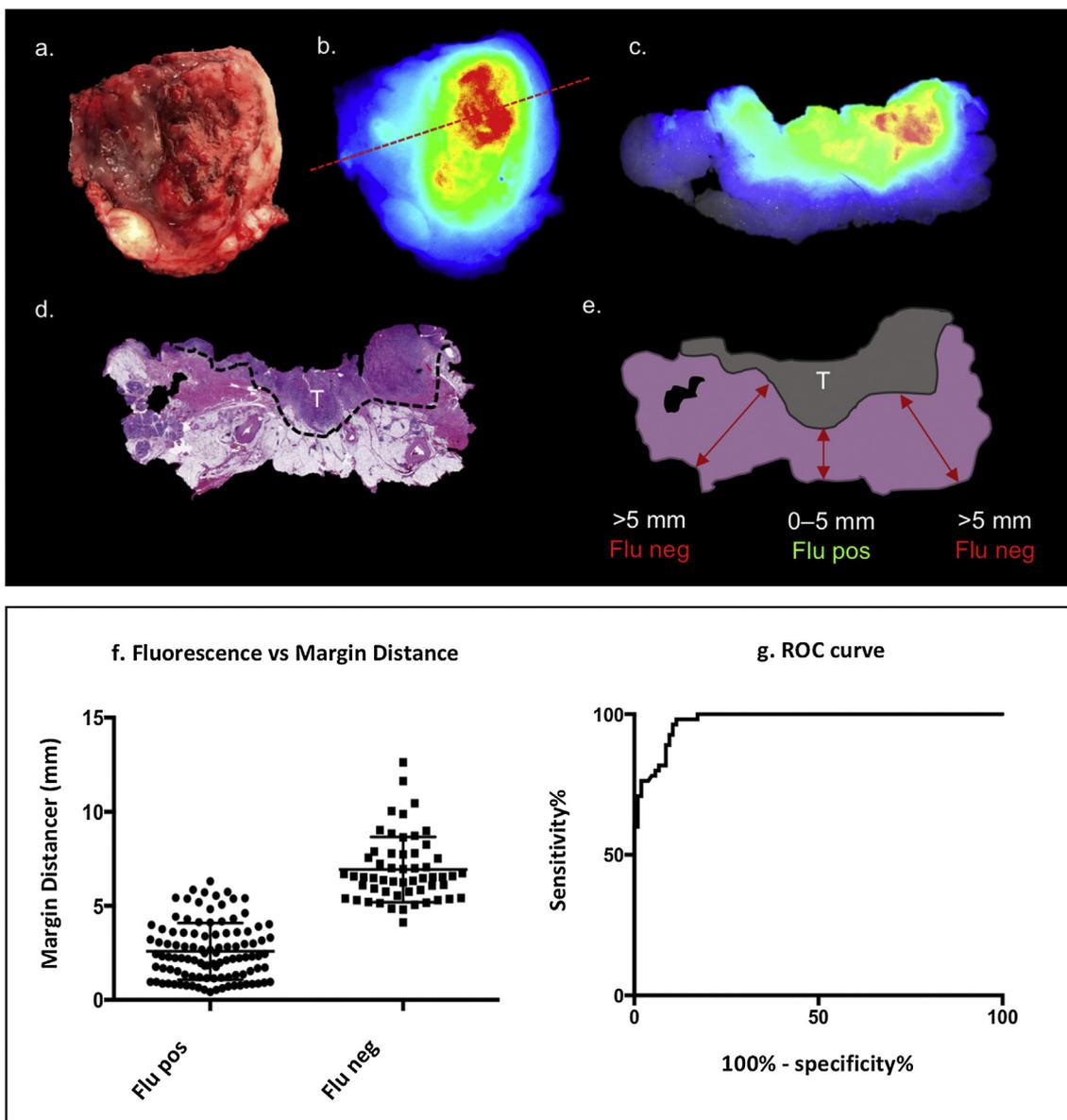
Fig. 5. Fluorescence signal versus *margin distance*. Bright field and corresponding fluorescence top view images of surgical specimen are shown (a and b). The red dashed line (b) indicates the position from where the 5 mm serial section (c) was obtained. The H&E slide (d) with delineated tumor (dashed black line) and corresponding illustration of the H&E slide (e). Quantitative analysis demonstrates a significant difference in tumor distance between fluorescence positive and negative areas. T = tumor; Flu neg = negative for fluorescence; Flu pos = positive for fluorescence; Margin distance = tumor-edge-to-specimen-edge distance.

sectioning. Our data suggests that fluorescence is highly sensitive to detect cancer within the clinically relevant cut-offs (< 2 mm and < 5 mm; 100% and 95%, respectively) and could be valuable as confirmation of a negative margin. When a margin is positive for fluorescence, the surgeon would have the opportunity to re-resect additional tissue at the suspicious area. This additional tissue can be imaged as well to assess fluorescence status and assure a negative margin. The 3D information from the specimen that details the location of close or positive margins becomes available to the surgeon immediately after resection and may provide important information that the surgeon can incorporate into decision making.

Here we use the unique properties of NIR light to our advantage; penetration of NIR light through normal soft-tissue (i.e. muscle and fat) is approximately 5–6 mm, and therefore can be used to select areas at risk for positive margins during imaging of the specimen. Consistent with the known properties of NIR light, we demonstrated the maximum penetration depth of panitumumab-IRDye800 being 6.3 mm whereby we reached > 95% sensitivity and specificity for identifying tumor

involved margins. Although variations in soft-tissue composition and signal intensity will certainly influence the depth of penetration, from a clinical perspective, a margin of greater than 5 mm is considered negative. This technique could ultimately identify areas that are suspicious for tumor within 5–6 mm of the specimen edge. If validated by clinical judgement or frozen section analysis as well, then the surgeon has the immediate opportunity to return to the wound bed to further resect that specific margin. This strategy would be more efficient, reduce sampling error and provide confidence and additional guidance for the operating surgeon.

We believe that due to limited exposure and challenging anatomy in patients with HNSCC, they particularly may benefit from closed-field OSM rather than intermittent *in situ* imaging, which is not always adapted easily into the surgical workflow. We have previously demonstrated that specimen imaging using a closed-field system to obtain quantitative fluorescence imaging information has distinct advantages [14,23,27]. However, a single planar image of the specimen had significant limitations and as a consequence we worked collaboratively to

develop the OSM device for complete imaging of all specimen surfaces. The OSM device performs nearly complete surface mapping in approximately 7 min, which allows immediate evaluation in the operating room. Importantly, the OSM imaging methods provide a quantitative and scalable image in high resolution, unlike open-field devices that are currently the standard of care for most surgical imaging.

While this study represents a successful first-in-human proof-of-concept of OSM, important limitations should be addressed. First and foremost, although many optimal imaging agents are currently being evaluated in late stage clinical trials [19,24,25,27], it will require the approval of a successful optical imaging agent for general use. Another limitation is inherent to the use of the OSM device, and directly relatable to fluorescence imaging: limited penetration depth and presence of autofluorescence. Although, the autofluorescence is strongly reduced and the penetration depth improved compared to visual fluorescence dyes, it is still limited compared to that of radiotracers [3].

Optical imaging strategies that identify tumor at the cut surface are appropriate for tumors deriving from the breast or the brain, but for lung, head and neck, colon and pancreas cancers the margin is considered close/positive within 5 mm of the tumor. Therefore, given the penetration depth of IRDye800, our proposed method might not be appropriate for breast and brain cancers, since fluorescence signal at the specimen edge might be detected up to 5–6 mm from the tumor edge. For these tumor types, one might consider a slightly different approach, such as visual fluorescent dyes (i.e. fluorescein isothiocyanate; penetration depth 1–2 mm). However, for tumor types in which a 5 mm margin is required, the relative high penetration depth of panitumumab-IRDye800 is a distinct advantage. If the margin appears clear on gross inspection and no fluorescence signal is observed, the margin should be considered not suspicious for tumor within 5 mm. The robustness for this proposed approach is validated in our cohort by the low false-negative rate (i.e. no fluorescence signal, and tumor within < 5 mm) of 2% and excellent sensitivity and specificity. Moreover, as we reduce the acceptable margin distance we find a corresponding decrease in the false negative rate with a corresponding reduction in the number of false-positive margins (decreased specificity). This is likely due to scatter of light within the soft-tissue. From a clinically relevant perspective, one would rather have a false-positive result than a false-negative result as leaving malignant tissue behind can have significant consequences for the patient [11,26]. Such a technique could significantly decrease our current poor margin control rate and thereby effectuate improved locoregional disease control and patient survival. In addition, due to the expression of EGFR by regional metastatic disease, we believe OSM also has potential for the identification of tumor-involved lymph nodes and this application is currently under evaluation.

Conclusion

Our proposed strategy using fluorescent OSM could have substantial advantage in rapidly and accurately assessing tumor margins in real-time. OSM can provide a highly sensitive method to detect cancer within 5 mm of the surgical margin and thereby assist the surgeon in judging completeness of resection or preselect areas of interest for further frozen sectioning analysis. The proposed technique of OSM, while optimal in HNSCC, would be very useful in many other cancers for which wide margin status is desired (e.g. lung and colorectal cancer). The data presented here supports further development of OSM as high priority.

Disclosures

H-W.W. and L.M. are employees of LI-COR Biosciences. E.L.R. acts as consultant for LI-COR Biosciences that manufactures IRDye800 and has equipment loans from this company. All other authors declare no conflict of interest.

References

[1] DeVita V, Hellman S, Rosenberg S. Cancer: principles and practice of oncology [internet]. 10th ed. Philadelphia: Wolters Kluwer; 2015.

[2] Roh J-L, Yeo N-K, Kim JS, Lee JH, Cho K-J, Choi S-H, et al. Utility of 2-[18F] fluoro-2-deoxy-d-glucose positron emission tomography and positron emission tomography/computed tomography imaging in the preoperative staging of head and neck squamous cell carcinoma. Oral Oncol 2007;43(9):887–93.

[3] Schaafsma BE, Verbeek FPR, Rietbergen DDD, van der Hiel B, van der Vorst JR, Liefers GJ, et al. Clinical trial of combined radio- and fluorescence-guided sentinel lymph node biopsy in breast cancer. Br J Sug 2013;100(8):1037–44.

[4] Catanzaro S, Copelli C, Manfuso A, Tewfik K, Pederneschi N, Cassano L, et al. Intraoperative navigation in complex head and neck resections: indications and limits. Int J Comput Assist Radiol Surg 2017;12(5):881–7.

[5] Tipirneni KE, Warram JM, Moore LS, Prince AC, de Boer E, Jani AH, et al. Oncologic procedures amenable to fluorescence-guided surgery. Ann Surg 2017;266(1):36–47.

[6] Woolgar JA, Triantafyllou A. A histopathological appraisal of surgical margins in oral and oropharyngeal cancer resection specimens. Oral Oncol 2005;41(10):1034–43.

[7] McMahon J, O'Brien CJ, Pathak I, Hamill R, McNeil E, Hammersley N, et al. Influence of condition of surgical margins on local recurrence and disease-specific survival in oral and oropharyngeal cancer. Br J Oral Maxillofac Surg 2003;41(4):224–31.

[8] Ravasz LA, Slootweg PJ, Hordijk GJ, Smit F, van der Tweel I. The status of the resection margin as a prognostic factor in the treatment of head and neck carcinoma. J Cranio-Maxillo-fac Surg 1991;19(7):314–8.

[9] Eldeeb H, Macmillan C, Elwell C, Hammod A. The effect of the surgical margins on the outcome of patients with head and neck squamous cell carcinoma: single institution experience. Canc Biol Med 2012;9(1):29–33.

[10] Pawlik TM, Scoggins CR, Zorzi D, Abdalla EK, Andres A, Eng C, et al. Effect of surgical margin status on survival and site of recurrence after hepatic resection for colorectal metastases. Ann Surg 2005;241(5):715–22. [discussion 722–724].

[11] Hinni ML, Ferlito A, Brandwein-Gensler MS, Takes RP, Silver CE, Westra WH, et al. Surgical margins in head and neck cancer: a contemporary review. Head Neck 2013;35(9):1362–70.

[12] Jaafar H. Intra-operative frozen section consultation: concepts, applications and limitations. Malays J Med Sci 2006;13(1):4–12.

[13] Ord RA, Aisner S. Accuracy of frozen sections in assessing margins in oral cancer resection. J Oral Maxillofac Surg 1997;55(7):663–9.

[14] Gao RW, Teraphongphom NT, van den Berg NS, Martin BA, Oberhelman NJ, Divi V, et al. Determination of tumor margins with surgical specimen mapping using near-infrared fluorescence. Canc Res 2018;78(17):5144–54.

[15] Rosenthal E, Moore L, Tipirneni K, de Boer E, Stevens TM, Hartman YE, et al. Sensitivity and specificity of cetuximab-IRDye800CW to identify regional metastatic disease in head and neck cancer. Clin Canc Res 2017;23(16):4744–52.

[16] Lamberts LE, Koch M, de Jong JS, Adams ALL, Glatz J, Kranendonk MEG, et al. Tumor-specific uptake of fluorescent bevacizumab-IRDye800CW microdosing in patients with primary breast cancer: a Phase I feasibility study. Clin Canc Res 2017;23(11):2730–41.

[17] Schaafsma BE, Mieog JSD, Hutteman M, van der Vorst JR, Kuppen PJK, Löwik CWGM, et al. The clinical use of indocyanine green as a near-infrared fluorescent contrast agent for image-guided oncologic surgery. J Surg Oncol 2011;104(3):323–32.

[18] Samkoe KS, Bates BD, Tselepidakis NN, DSouza AV, Gunn JR, Ramkumar DB, et al. Development and evaluation of a connective tissue phantom model for subsurface visualization of cancers requiring wide local excision. J Biomed Opt 2017;22(12):1–12.

[19] Gao RW, Teraphongphom N, de Boer E, van den Berg NS, Divi V, Kaplan MJ, et al. Safety of panitumumab-IRDye800CW and cetuximab-IRDye800CW for fluorescence-guided surgical navigation in head and neck cancers. Theranostics 2018;8(9):2488–95.

[20] Day KE, Beck LN, Deep NL, Kovar J, Zinn KR, Rosenthal EL. Fluorescently labeled therapeutic antibodies for detection of microscopic melanoma. Laryngoscope 2013;123(11):2681–9.

[21] Day KE, Beck LN, Heath CH, Huang CC, Zinn KR, Rosenthal EL. Identification of the optimal therapeutic antibody for fluorescent imaging of cutaneous squamous cell carcinoma. Cancer Biol Ther 2013;14(3):271–7.

[22] Day KE, Sweeny L, Kulbersh B, Zinn KR, Rosenthal EL. Preclinical comparison of near-infrared-labeled cetuximab and panitumumab for optical imaging of head and neck squamous cell carcinoma. Mol Imag Biol 2013;15(6):722–9.

[23] Rosenthal EL, Warram JM, de Boer E, Chung TK, Korb ML, Brandwein-Gensler M, et al. Safety and tumor-specificity of cetuximab-IRDye800 for surgical navigation in

head and neck cancer. Clin Canc Res 2015;21(16):3658–66.

[24] Jichlinski P, Guillou L, Karlsen SJ, Malmström P-U, Jocham D, Brennhovd B, et al. Hexyl aminolevulinate fluorescence cystoscopy: new diagnostic tool for photo-diagnosis of superficial bladder cancer – a multicenter study. J Urol 2003;170(1):226–9.

[25] van den Berg NS, Simon H, Kleinjan GH, Engelen T, Bunschoten A, Welling MM, et al. First-in-human evaluation of a hybrid modality that allows combined radio- and (near-infrared) fluorescence tracing during surgery. Eur J Nucl Med Mol Imag 2015;42(11):1639–47.

[26] Cook JA, Jones AS, Phillips DE, Soler Lluch E. Implications of tumour in resection margins following surgical treatment of squamous cell carcinoma of the head and neck. Clin Otolaryngol Allied Sci 1993;18(1):37–41.

[27] Lamberts LE, Koch M, de Jong JS, Adams ALL, Glatz J, Kranendonk MEG, et al. Tumor-specific uptake of fluorescent bevacizumab-irdye800cw microdosing in pa-tients with primary breast cancer: a phase I feasibility study. Clin Cancer Res 2017;23(11):2730–41.